EUROPEAN ORGANIZATION FOR NUCLEAR RESEARCH

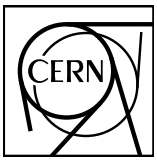

CERN-EP-2018-XXX
6 September 2018

Jet fragmentation transverse momentum measurements correlations in $\sqrt{s_{\rm NN}} = 5.02$ TeV p–Pb collisions

ALICE Collaboration*

Abstract

Jet fragmentation transverse momentum ($j_{\rm T}$) distributions are measured using full jet reconstruction in proton-lead (p–Pb) collisions at $\sqrt{s_{\rm NN}} = 5.02$ TeV with the ALICE experiment at the LHC. Jets are reconstructed using the anti-kT algorithm with resolution parameter $R = 0.4$ in the pseudorapidity range $|\eta| < 0.25$. The $j_{\rm T}$ values are calculated for the charged tracks inside the jet cone around the jet axis. The measured distributions show a clear narrow Gaussian component and a wide component described by an inverse gamma function. In previous studies the narrow component is related to hadronization and the wide component to the showering process. The width of the wide component increases with increasing jet transverse momentum, while the width of the narrow component has only a weak dependance on jet momentum. The results are compared to PYTHIA and Herwig simulations, showing that trends in data are successfully described by them. The $j_{\rm T}$ distributions in the high multiplicity p–Pb collisions is compared to the minimum bias collisions, indicating there is no strong jet modification while the significant elliptic flow was observed in those events.

*See Appendix A for the list of collaboration members

1 Introduction

Jets are collimated sprays of hadrons originating from the fragmentation of hard partons produced in high-energy particle collisions. Studying the jet fragmentation can give insight into Quantum Chromodynamics (QCD) [1–5] phenomena, such as angular ordering [6] and the color-neutralization process known as hadronization [7–9]. In this work the fragmentation of partons is studied using the jet fragmentation transverse momentum, j_{T}, which is the perpendicular component of the momentum with respect to the momentum vector of the initial hard parton.

Previously, j_{T} has been studied using two-particle correlations by the CCOR collaboration at ISR in pp collisions at center-of-mass energy $\sqrt{s} = 31$, 45 and 63 GeV [10] and the PHENIX collaboration at RHIC in pp collisions at $\sqrt{s} = 200$ GeV [11] and d–Au collisions at center-of-mass energy per nucleon pair $\sqrt{s_{\mathrm{NN}}} = 200$ GeV [12]. Jet measurements to study j_{T} have been done by the CDF collaboration at the Tevatron in $\mathrm{p\bar{p}}$ collisions at $\sqrt{s} = 1.96$ TeV [13] and the ATLAS collaboration at the LHC in Pb–Pb collisions at $\sqrt{s_{\mathrm{NN}}} = 2.76$ TeV [14]. Jet production in QCD can be thought of as two separate stages [15]. After being produced in the hard scattering, partons reduce their high virtuality through emitting gluons. Since the transverse momentum scale (Q^2) is large during the showering, perturbative QCD calculations can be applied. When Q^2 becomes of the order of Λ_{QCD}, partons hadronize into final-state particles through a non-perturbative process.

As non-perturbative processes these are hard to calculate from first principles. Instead Monte Carlo generators such as PYTHIA [7] and Herwig [9] are used to produce a theoretical background. One approach based on perturbative QCD (pQCD) is the Next-to-Modified Leading Log Approximation (NMLLA) [16]. This approach implements local parton hadron duality (LPHD) [17] instead of any sophisticated hadronisation model.

These two MC generators handle both the showering process and hadronisation differently. Pythia uses the Lund string model [18] to perform the hadronisation stage. Herwig uses a cluster model for the hadronisation. Pythia 6 has p_{T} ordered showers while Pythia 8 has rapidity ordered showers. Herwig simulates parton showers using the coherent branching algorithm of [19]. This algorithm has angular ordering as a central feature. In PYTHIA 8 angular ordering is built in, while in PYTHIA 6 it can be turned on or off.

Jets also are used as an important probe for the study of the deconfined phase of strongly interacting QCD matter, the quark-gluon plasma (QGP) that is created in high energy collisions of heavy nuclei. There have been many experimental evidences of jet energy loss, such as the suppression of inclusive hadron spectra at high transverse momentum [20–24], the modification of back-to-back hadron-hadron [25, 26] and direct photon-jet correlations [27], and the modification of reconstructed jet spectra [28] and jet substructure [29–31], as compared to the expectations from elementary proton-proton collisions.

Jet quenching in heavy-ion collisions evolves multi-scale problems [32, 33]. The elementary scattering and the subsequent branching process down to non-perturbative scales are dominated by hard scales in the vacuum as well as in the medium. Soft scales, of the order of the temperature of the medium, characterise the interactions of soft partons produced in the shower with the QGP. Soft scales also rule hadronisation, which is expected to take place in vacuum for sufficiently energetic probes. Understanding the contributions from the different processes to the jet shower evolution in medium and their scale dependence is crucial to to constrain the dynamics of jet energy loss in the expending medium, the role of colour coherence [34], and fundamental medium properties like temperature dependent transport coefficient [35, 36].

The observed strong collective behavior suggests that the QGP is created in high multiplicity pp and pA collisions [37–42], even though in order to reach a final conclusion more experimental and theoretical efforts are required. Jet production could be modified even if the collision system is small [43–45], though

no clear consensus on the magnitude of the quenching has been made. There had been no evidence of jet quenching in minimum bias collisions [23, 46], i.e. averaged over all events. However, in these small systems, the selection of event class based on multiplicity has strong autocorrelations between the nature of the nucleon-nucleon collisions and the hard process itself. This makes the interpretation of experimental observables complicated [47–49] because the measurements are limited on the cross section of high-p_{T} hadrons and jets to date.

The results for j_{T} distributions by using two-particle correlations were recently reported by the ALICE Collaboration [46]. It was demonstrated that j_{T} distributions have two distinct components related to the showering and hadronization phases. The advantage of jet reconstruction is that it should give a better estimate of the initial hadron momentum when compared to using two-particle correlations. Additionally the results are not smeared by the splitting of the leading hadron as was the case in the correlation study. The disadvantage is that the jet reconstruction limits the study to a small cone around the jet axis. Additionally the kinematics of produced jets are different. In wo-particle correlations, the results are done in p_{Ttrigger} bins, which favored harder jets (leading track carries a large fraction of the momentum). When looking at p_{Tjet} bins softer jets are favored.

In this paper, the j_{T} distributions are studied by reconstructing the jets using the anti-kT algorithm with resolution parameter $R = 0.4$ in the pseudorapidity range $|\eta| < 0.25$ [50] in $\sqrt{s_{\mathrm{NN}}} = 5.02$ TeV p–Pb minimum bias and high multiplicity collisions. Two distinct components are studied for various jet transverse momentum bins and event selections. We also present a comparison to PYTHIA and Herwig simulations.

The experimental setup and measurements are described in Sec. 2. In Sec. 3 we present the analysis methods. The sources of systematic uncertainties are explained in Sec. 4. The results of the measurements and comparisons to model calculations are presented in Sec. 5. Finally, Sec. 6 summarizes our new results.

2 Experimental setup and data samples

The $\sqrt{s_{\mathrm{NN}}} = 5.02$ TeV p–Pb ($1.3 \cdot 10^8$ events, $\mathscr{L}_{\mathrm{int}} = 620\,\mathrm{nb}^{-1}$) collisions were recorded in 2013 by the ALICE detector [51]. The details of the performance of the ALICE detector during LHC Run 1 (2009-2013) are presented in Ref. [52].

The analysis uses charged tracks that are reconstructed with the Inner Tracking System (ITS) [53] and the Time Projection Chamber (TPC) [54]. These detectors are located inside the large solenoidal magnet, that provides a homogeneous magnetic field of 0.5 T. Tracks within a pseudorapidity range $|\eta| < 0.9$ over the full azimuth can be reconstructed. The ITS is made up of the innermost Silicon Pixel Detector (SPD), the Silicon Drift Detector (SDD) and the outermost Silicon Strip Detector (SSD). Each of these consists of two layers. The TPC is a cylinder filled with gas. Gas is ionised along the path of charged particles. Liberated electrons drift towards the end plates of the cylinder where they are detected. Combining the information from the ITS and the TPC provides a resolution ranging from 1 to 10 % for charged particles with momenta from 0.15 to 100 GeV/c. For tracks without the ITS information, the momentum resolution is comparable to that of ITS+TPC tracks below transverse momentum $p_{\mathrm{T}} = 10\,\mathrm{GeV/c}$, but for higher momenta the resolution reaches 20 % at $p_{\mathrm{T}} = 50\,\mathrm{GeV/c}$ [52, 55].

Neutral particles used in jet reconstruction are reconstructed by the Electromagnetic Calorimeter (EMCAL) [56]. The EMCAL covers an area with a range of $|\eta| < 0.7$ in pseudorapidity and 100 deg in azimuth. EMCAL is complimented with the Dijet Calorimeter (DCal) [57] and Photon Spectrometer (PHOS) [58] that are situated opposite of the EMCAL in azimuth. PHOS covers 70 degrees in azimuth and $|\eta| < 0.12$. The DCal is technologically identical to EMCal. The DCal coverage spans over 67 degrees in azimuth, but in pseudorapidity the mid region is occupied by the PHOS. In between PHOS

and DCal active volumes, there is a gap of 10 cm. DCal is fully back-to-back with EMCal.

The combination of charged tracks with $p_{\mathrm{T}} > 0.15\,\mathrm{GeV/c}$ and neutral particles with $p_{\mathrm{T}} > 0.30\,\mathrm{GeV/c}$ is used to construct jets.

The V0 detector [59] provides the information for event triggering. The V0 detector consists of two scintillator hodoscopes that are located on either side of the interaction point along the beam direction. It covers the pseudorapidity region $-3.7 < \eta < -1.7$ (V0C) and $2.8 < \eta < 5.1$ (V0A). For the 2013 p–Pb collisions events are required to have signals in both V0A and V0C. This condition is used later offline to reduce the contamination of the data sample from beam-gas events by using the timing difference of the signal between the two stations [52].

EMCAL is also used to provide the jet trigger used in triggered datasets. EMCAL can be used to trigger on single shower deposits or energy deposits integrated over a larger area. Latter case is used for jet triggers. The EMCAL trigger definition in the 2013 p–Pb collisions requires an energy deposit of either 10 GeV for the low threshold trigger or 20 GeV for the high threshold trigger in a 32×32 patch size.

In p–Pb collisions the tracks are selected following the hybrid approach [60] which ensures a uniform distribution of tracks as a function of azimuthal angle (φ). The momentum resolutions of the two classes of particles are comparable up to $p_{\mathrm{T}} \approx 10\,\mathrm{GeV}/c$, but after that, tracks without ITS requirements have a worse resolution [52, 55].

3 Analysis method

The analysis is performed by analysing jet constituents. In each collision event, the jets are reconstructed using FastJet [61] with the anti-k_{T} algorithm [50]. Jets for R=0.4 are selected in $|\eta| < 0.25$ to satisfy the fiducial acceptance of the EMCal. In jet reconstruction both charged tracks with $p_{\mathrm{T}} > 0.15\,\mathrm{GeV/c}$ and neutral cluster with $p_{\mathrm{T}} > 0.30\,\mathrm{GeV/c}$ are considered. In the analysis, results are presented in terms of the jet transverse momentum p_{Tjet}.

The jet fragmentation transverse momentum, j_{T}, is defined as the component of the constituent particle momentum, $\vec{p}_{\mathrm{a}}$, transverse to the jet momentum, $\vec{p}_{\mathrm{jet}}$. The length of the $\vec{j}_{\mathrm{T}}$ vector is

$$j_{\mathrm{T}} = \frac{|\vec{p}_{\mathrm{jet}} \times \vec{p}_{\mathrm{track}}|}{|\vec{p}_{\mathrm{jet}}|}\,. \tag{1}$$

It is commonly interpreted as a transverse kick with respect to the initial hard parton momentum that is given to a fragmenting particle during the fragmentation process, which is a measure of the momentum spread of the jet fragments [].

The reconstructed jet axis is used for j_{T} reference. Any charged track within a fixed cone with radius R is taken as a jet constituent, as opposed to using the constituent list provided by the jet algorithm. Anti-k_{T} produces jets that are very circular in shape. Thus this doesn't change the constituent list considerably. Neutral tracks are used only in jet reconstruction.

The resulting j_{T} distributions are corrected for the detector inefficiency using the unfolding method. The response matrix for the unfolding is obtained from a PYTHIA [7]+GEANT [62, 63] simulation.

The underlying event is estimated by looking at an imaginary jet cone perpendicular to the observed jet axis ($\frac{\pi}{2}$ Rotation in ϕ). j_{T} is calculated for any tracks found within this cone. The vector sum of the individual track momentum and the imaginary jet axis is used as reference for j_{T}. The background obtained in this manner is subtracted from the unfolded inclusive j_{T} distribution, which gives the resulting signal distribution. To make sure there is no jet contribution in the background, any events with jets inside the perpendicular cone are not used for background estimation.

The resulting signal distribution are fitted with a 2 component function shown in Eq. 2. Gaussian distribution is used for low j_{T} and an inverse gamma function is used for high j_{T}. The gaussian is taken to have the center at $j_{\mathrm{T}} = 0$. In total this gives 5 parameters. [46]

$$\frac{1}{N_{\mathrm{jets}}}\frac{\mathrm{d}N}{j_{\mathrm{T}}\mathrm{d}j_{\mathrm{T}}} = \frac{B_2}{B_1\sqrt{2\pi}}e^{-\frac{j_{\mathrm{T}}^2}{2B_1^2}} + \frac{B_3 B_5^{B_4}}{\Gamma(B_4)}\frac{e^{-\frac{B_5}{j_{\mathrm{T}}}}}{j_{\mathrm{T}}^{B_4+1}} \tag{2}$$

To achieve stable results the fitting is performed in two steps. First each component is fitted separately. Gaussian component is fitted to the low end in j_{T}. Inverse gamma component is fitted to j_{T} above $1\,\mathrm{GeV/c}$. After getting the results from the individual fits they are combined into a single function with initial values from the individual results and an additional fit is performed. The result from fitting only the gaussian component to the entire distribution is approximately the same as the gaussian component in the two-component model.

After getting the fit function $\sqrt{\langle j_{\mathrm{T}}^2\rangle}$ (RMS) and yield values are extracted separately from each component. The narrow component RMS is

$$\sqrt{\langle j_{\mathrm{T}}^2\rangle} = \sqrt{2}B_1,$$

and the wide component RMS value is calculated as

$$\sqrt{\langle j_{\mathrm{T}}^2\rangle} = \frac{B_5}{\sqrt{(B_4-2)(B_4-3)}},$$

where it is required that $B_4 > 3$.

4 Systematic uncertainties

The systematic uncertainties in this analysis come from the background estimation, the unfolding procedure and the cuts used to select the tracks. Tracking uncertainties are estimated from variations of the track selection cuts defined in Sec. 2. The resulting variations in RMS are shown in Table 1. The uncertainties from unfolding and background subtraction are of the same magnitude.

The systematics in background estimation were studied using an alternative method to extract the background, mainly the random background method. The resulting uncertainty is below 5% for the wide component RMS and below 9% for the narrow component RMS.

The systematic uncertainty that arises from the unfolding procedure is estimated by performing the unfolding with two separate methods. Data corrected by the iterative unfolding method are used as the results and the SVD unfolding method is employed to estimate the uncertainty. In a PYTHIA closure test the true distribution was in general found to be between the unfolded distributions from the iterative and SVD method. The difference between the methods when unfolding data should give a reasonable estimate of the unfolding uncertainty. The resulting uncertainty is below 8% for both wide and narrow component RMS.

The different source of the systematic uncertainty are considered as uncorrelated and the values of each source are summed in quadrature. The resulting uncertainty is 9 % for the wide component RMS and 12 % for the narrow component RMS.

There is no tracking and no unfolding uncertainty in the Monte Carlo simulations.

Table 1: Summary of systematic errors

Systematic	Wide RMS	Narrow RMS
Background	5 %	9 %
Unfolding	8 %	8 %
Tracking	? %	? %
Total	9 %	12%

5 Results

Distributions of j_{T} after unfolding and background subtraction are shown in Fig. 1. The yield at low j_{T} stays constant with increasing p_{Tjet}. At high j_{T} the yield increases and the distributions become wider. In part this is due to kinematical limits. Within a fixed cone the maximum j_{T} depends on the track momentum.

$$j_{\mathrm{Tmax}} \approx R \cdot p_{\mathrm{Ttrack}}$$

With increasing jet p_{T} the possible track momenta also increase.

The distributions are fitted using a two component fit. An example of the fitted distribution is shown in Fig. **??**. The j_{T} distributions are well described by the two component model fit.

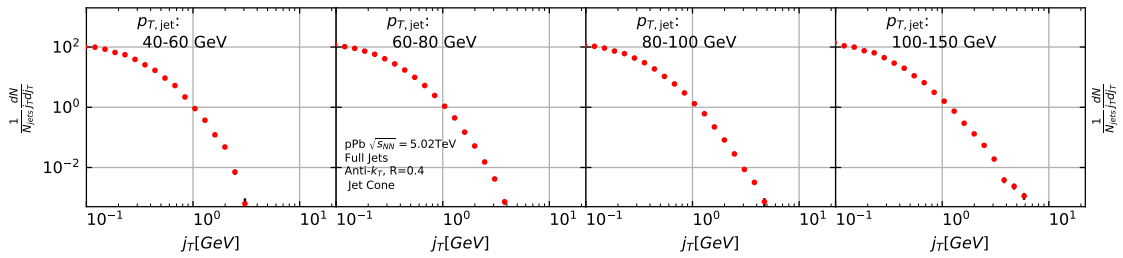

Figure 1: j_{T} distributions in different jet p_{T} bins.

The per jet yields and widths of the j_{T} distributions are determined as a function of the transverse momentum of jet. The results are obtained from the area and RMS of the fits to the narrow and wide components of the j_{T} distribution. The RMS $\left(\sqrt{\langle j_{\mathrm{T}}^2 \rangle}\right)$ values for the narrow component are shown in Fig. **??** with comparison to Monte Carlo simulations.

There is clear separation in the width of the wide and narrow components of the j_{T} distributions. The RMS of the wide component is 3-4 times larger than the narrow component RMS. The wide component is assumed to correspond to the fragmentation part of jet formation while the narrow component is linked with the hadronisation phase.

The wide component RMS shows an increasing trend with increasing p_{Tjet}, while the narrow component RMS stays roughly constant. Both of these trends are qualitatively consistent with the results seen in dihadron j_{T} analysis [46]

PYTHIA describes well the RMS values in both the narrow and wide components. Herwig...(insert observations from Herwgig) PYTHIA uses the Lund string model for hadronisation while Herwig uses a cluster model. It seems ...

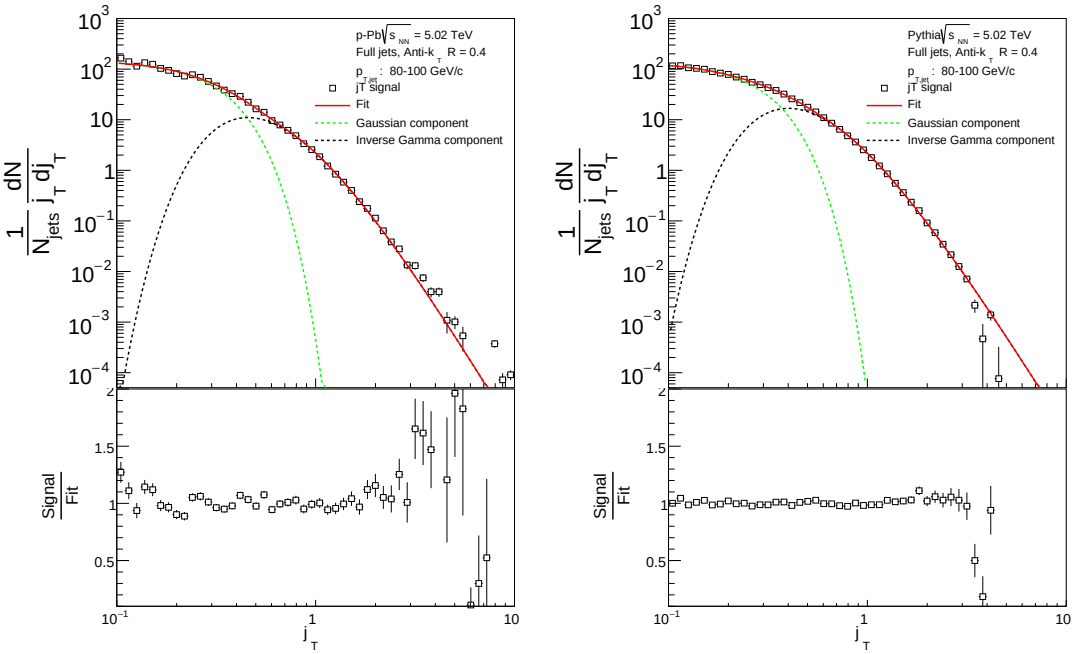

Figure 2: j_T distribution with two component fitting

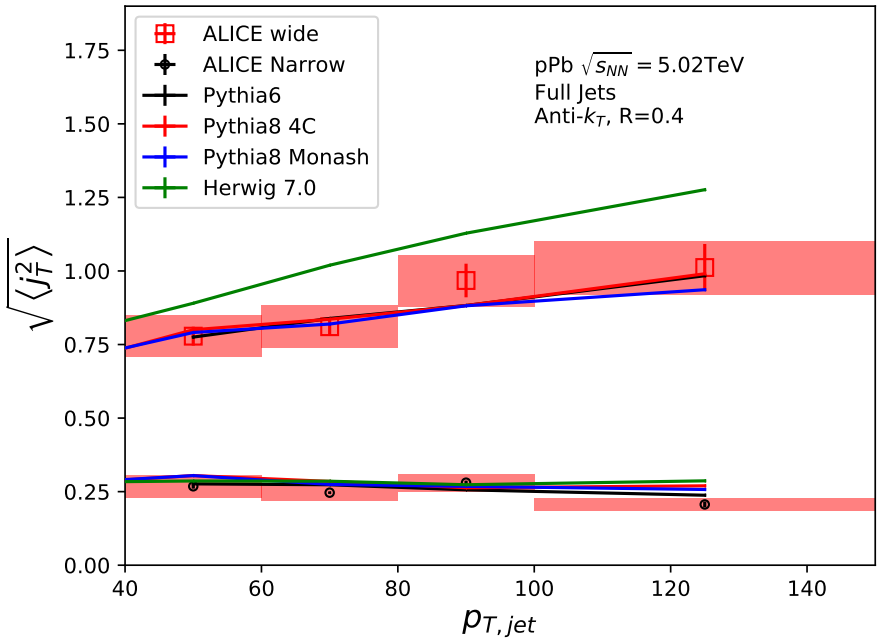

Figure 3: RMS and yield values extracted from the fits for the gaussian (narrow) and inverse gamma (wide) components

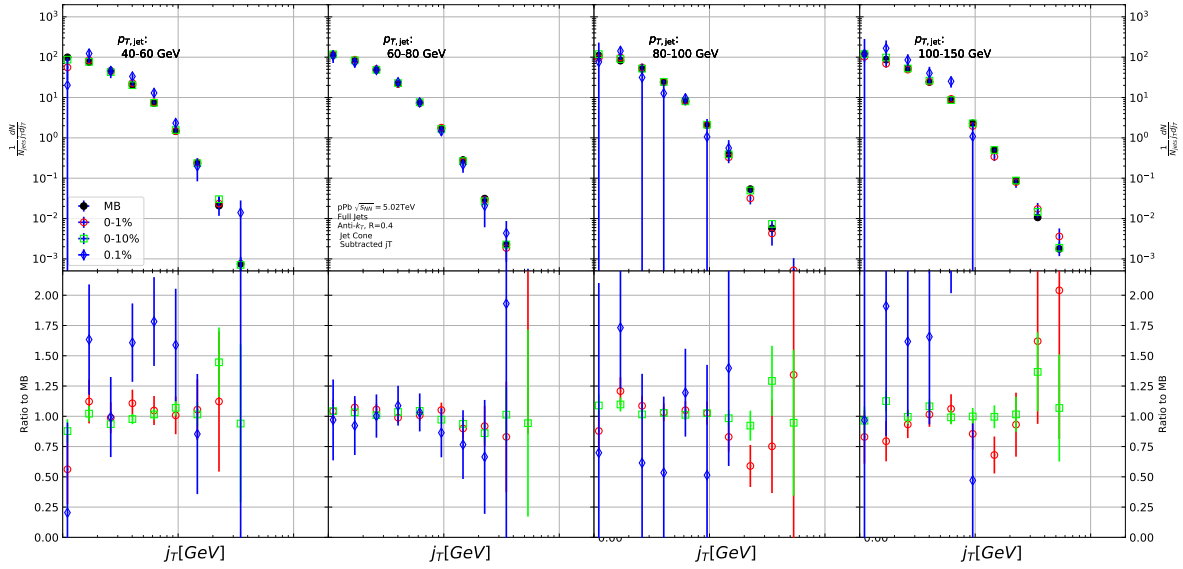

Figure 4: High multiplicity events

5.1 Discussions

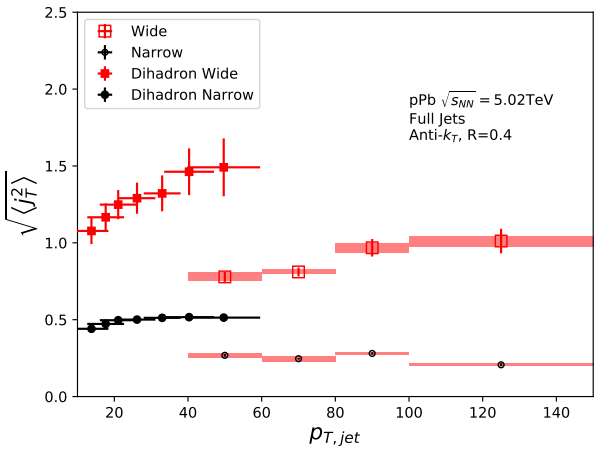

Figure 5: Comparison of results with dihadron j_T results. Dihadron trigger p_T bins are converted to jet p_T bins using observed mean p_{Tjet} values in $p_{Ttrigger}$ bins. Dihadron results are for $0.2 < x_{||} < 0.4$

Comparison to j_T results from dihadron analysis [46] is shown in Fig. 5. Trigger p_T bins used in dihadron analysis are converted to jet p_T bins using observed average jet p_T values in leading track momentum bins. Simlarly jet p_T bins are converted to $p_{Ttrigger}$ bins using average leading track p_T values in p_{Tjet} bins.

The trends are similar in dihadron and jet j_T results. Wide component RMS values tend to increase with increasing $p_{Ttrigger}/p_{Tjet}$. Narrow component RMS increases slightly in dihadron analysis but not in jet j_T, WHY? (Depends on $x_{||}$ bin in dihadron)

In general dihadron j_T gives wider distributions with larger RMS values. In jet analysis the cone size limits width and thus the RMS values. With increasing cone size one gets increasing wide RMS values as seen in Fig. 6. This should be the dominant factor.

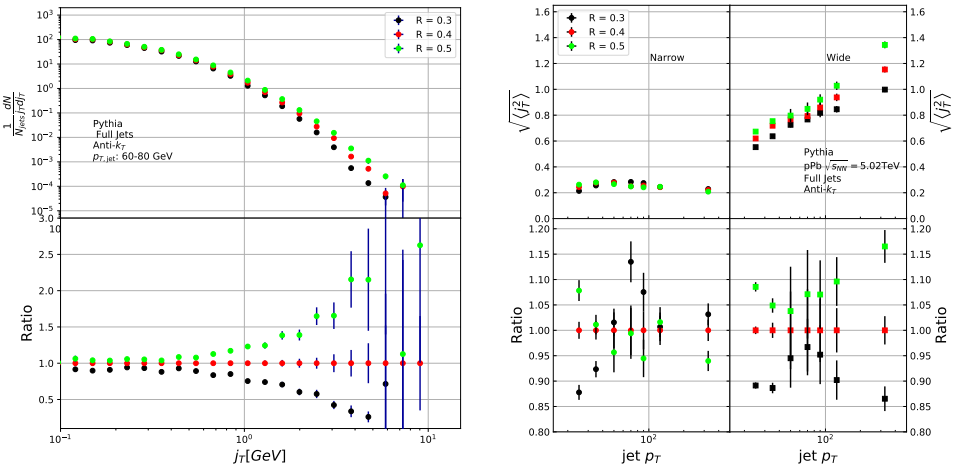

Figure 6: Effect of changing R parameter in jet finding on j_T distributions

Effect of the R parameter choice is studied in PYTHIA. Having a fixed cone puts hard limits on the possible j_T values. Increasing the cone size loosens these limits and allows higher j_T values. The results are shown in Fig. 6. Left hand side shows the j_T distributions. There is very little change in low j_T but at high j_T the yield increases.

This is also seen in the RMS values shown in the right hand side of Fig. 6, where the change in wide component RMS is about 10% when going from $R = 0.4$ to $R = 0.3$ or $R = 0.5$. With the narrow component values the situation is less clear. At low jet p_{T} larger R parameter leads to larger RMS values, but at hight p_{Tjet} the situation is reversed; increasing the R parameter decreases RMS values.

Additionally the leading track is an imperfect estimate of the jet/original parton. Because the leading track in general is at an angle compared to the jet axis, the resulting j_{T} values are different. In practice the jet axis found by the jet finding algrorithm tends to minimize the average j_{T} of jet constituents. Thus the yield at high j_{T} is limited and the RMS values are smaller.

A PYTHIA study was performed where j_{T} was calculated with respect to the leading track momentum, instead of the jet axis. The results are shown in Fig. 7. The resulting j_{T} distributions are significantly wider than j_{T} distributions from the typical method. The effect seems to be larger than the effect seen in comparing different R values.

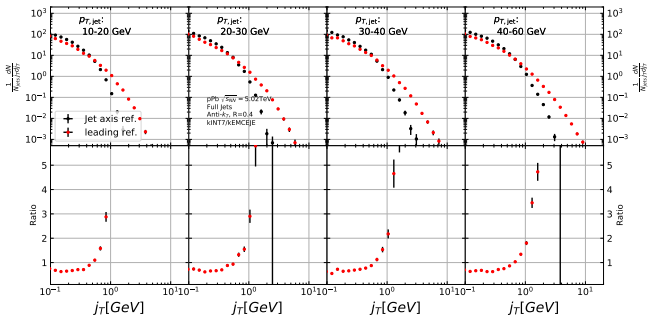

Figure 7: Results of calculating j_{T} with respect to the jet axis or the leading hadron. The assumption is that because the leading hadron is an imperfect estimate of the jet axis, low j_{T} tracks should on average be shifted to higher j_{T}

6 Summary

In this work two distinct j_{T} components were extracted for narrow and wide contributions using jet reconstruction. RMS values for both components were obtained. The width of the wide component is found to increase for increasing p_{Tjet}. This is in part explained by the changing kinematical limits when going to higher p_{Tjet} which allows higher p_{Ttrack}. Additionally the larger phase space allows stronger parton splitting. The results are qualitatively compatible with previous studies that studied j_{T} using two-particle correlations.

Acknowledgements

References

[1] D. J. Gross and F. Wilczek, "Ultraviolet behavior of non-abelian gauge theories," *Physical Review Letters* **30** no. 26, (1973) 1343–1346.

[2] H. D. Politzer, "Reliable perturbative results for strong interactions?," *Physical Review Letters* **30** no. 26, (1973) 1346–1349.

[3] D. J. Gross and F. Wilczek, "Asymptotically free gauge theories. i," *Physical Review D* **8** no. 10, (1973) 3633.

[4] D. J. Gross and F. Wilczek, "Asymptotically free gauge theories. ii," *Physical Review D* **9** no. 4, (1974) 980.

[5] H. Georgi and H. D. Politzer, "Electroproduction scaling in an asymptotically free theory of strong interactions," *Physical Review D* **9** no. 2, (1974) 416.

[6] Y. L. Dokshitzer, V. A. Khoze, A. H. Müller, and S. I. Troian, *Basics of Perturbative QCD*. Editions Frontières, Gif-sur-Yvette, France, 1991.

[7] T. Sjöstrand, S. Mrenna, and P. Z. Skands, "A Brief Introduction to PYTHIA 8.1," *Comput. Phys. Commun.* **178** (2008) 852–867, arXiv:0710.3820 [hep-ph].

[8] M. Bahr *et al.*, "Herwig++ Physics and Manual," *Eur. Phys. J.* **C58** (2008) 639–707, arXiv:0803.0883 [hep-ph].

[9] J. Bellm *et al.*, "Herwig 7.0/Herwig++ 3.0 release note," *Eur. Phys. J.* **C76** no. 4, (2016) 196, arXiv:1512.01178 [hep-ph].

[10] **CCOR** Collaboration, A. Angelis *et al.*, "A Measurement of the Transverse Momenta of Partons, and of Jet Fragmentation as a Function of $\sqrt{s}$ in pp Collisions," *Phys. Lett.* **B97** (1980) 163–168.

[11] **PHENIX** Collaboration, S. S. Adler *et al.*, "Jet properties from dihadron correlations in p+p collisions at $\sqrt{s} = 200$ GeV," *Phys. Rev.* **D74** (2006) 072002, arXiv:hep-ex/0605039 [hep-ex].

[12] **PHENIX** Collaboration, S. S. Adler *et al.*, "Jet structure from dihadron correlations in d+Au collisions at s(NN)**(1/2) = 200-GeV," *Phys. Rev.* **C73** (2006) 054903, arXiv:nucl-ex/0510021 [nucl-ex].

[13] **CDF** Collaboration, T. Aaltonen *et al.*, "Measurement of the k_T Distribution of Particles in Jets Produced in $p\bar{p}$ Collisions at $\sqrt{s} = 1.96$-TeV," *Phys. Rev. Lett.* **102** (2009) 232002, arXiv:0811.2820 [hep-ex].

[14] **ATLAS** Collaboration, A. Angerami, "Measurement of Jets and Jet Suppression in $\sqrt{s_{NN}} = 2.76$ TeV Lead-Lead Collisions with the ATLAS detector at the LHC," *J. Phys.* **G38** (2011) 124085, arXiv:1108.5191 [nucl-ex].

[15] A. Buckley *et al.*, "General-purpose event generators for LHC physics," *Phys. Rept.* **504** (2011) 145–233, arXiv:1101.2599 [hep-ph].

[16] R. Pérez-Ramos, F. Arleo, and B. Machet, "Next-to-modified leading logarithmic approximation corrections to single inclusive k_t distributions and two-particle correlations in a jet," *Physical Review D - PHYS REV D* **78** (07, 2008) 014019–014019.

[17] Y. I. Azimov, Y. L. Dokshitzer, V. A. Khoze, and S. I. Troyan, "Similarity of Parton and Hadron Spectra in QCD Jets," *Z. Phys.* **C27** (1985) 65–72.

[18] B. Andersson, G. Gustafson, G. Ingelman, and T. Sjöstrand, "Parton Fragmentation and String Dynamics," *Phys.Rept.* **97** (1983) 31–145.

[19] S. Gieseke, P. Stephens, and B. Webber, "New formalism for QCD parton showers," *JHEP* **12** (2003) 045, arXiv:hep-ph/0310083 [hep-ph].

[20] **PHENIX** Collaboration, K. Adcox *et al.*, "Suppression of hadrons with large transverse momentum in central Au+Au collisions at $\sqrt{s_{NN}}$ = 130-GeV," *Phys. Rev. Lett.* **88** (2002) 022301, arXiv:nucl-ex/0109003 [nucl-ex].

[21] **STAR** Collaboration, J. Adams *et al.*, "Evidence from d + Au measurements for final state suppression of high p(T) hadrons in Au+Au collisions at RHIC," *Phys. Rev. Lett.* **91** (2003) 072304, arXiv:nucl-ex/0306024 [nucl-ex].

[22] **BRAHMS** Collaboration, I. Arsene *et al.*, "Transverse momentum spectra in Au+Au and d+Au collisions at s**(1/2) = 200-GeV and the pseudorapidity dependence of high p(T) suppression," *Phys. Rev. Lett.* **91** (2003) 072305, arXiv:nucl-ex/0307003 [nucl-ex].

[23] **CMS** Collaboration, V. Khachatryan *et al.*, "Charged-particle nuclear modification factors in PbPb and pPb collisions at $\sqrt{s_{\mathrm{N\,N}}} = 5.02$ TeV," *JHEP* **04** (2017) 039, arXiv:1611.01664 [nucl-ex].

[24] **ALICE** Collaboration, S. Acharya *et al.*, "Transverse momentum spectra and nuclear modification factors of charged particles in pp, p-Pb and Pb-Pb collisions at the LHC," *JHEP* **11** (2018) 013, arXiv:1802.09145 [nucl-ex].

[25] **PHENIX** Collaboration, A. Adare *et al.*, "Transverse momentum and centrality dependence of dihadron correlations in Au+Au collisions at s(NN) = 200-GeV: Jet-quenching and the response of partonic matter," *Phys. Rev.* **C77** (2008) 011901, arXiv:0705.3238 [nucl-ex].

[26] **ALICE** Collaboration, K. Aamodt *et al.*, "Particle-yield modification in jet-like azimuthal di-hadron correlations in Pb-Pb collisions at $\sqrt{s_{NN}} = 2.76$ TeV," *Phys. Rev. Lett.* **108** (2012) 092301, arXiv:1110.0121 [nucl-ex].

[27] **PHENIX** Collaboration, A. Adare *et al.*, "Medium modification of jet fragmentation in Au + Au collisions at $\sqrt{s_{NN}} = 200$ GeV measured in direct photon-hadron correlations," *Phys. Rev. Lett.* **111** no. 3, (2013) 032301, arXiv:1212.3323 [nucl-ex].

[28] **ALICE** Collaboration, J. Adam *et al.*, "Measurement of jet suppression in central Pb-Pb collisions at $\sqrt{s_{\mathrm{NN}}}$ = 2.76 TeV," *Phys. Lett.* **B746** (2015) 1–14, arXiv:1502.01689 [nucl-ex].

[29] **CMS** Collaboration, A. M. Sirunyan *et al.*, "Observation of Medium-Induced Modifications of Jet Fragmentation in Pb-Pb Collisions at $\sqrt{s_{NN}} = 5.02$ TeV Using Isolated Photon-Tagged Jets," *Phys. Rev. Lett.* **121** no. 24, (2018) 242301, arXiv:1801.04895 [hep-ex].

[30] **CMS** Collaboration, S. Chatrchyan *et al.*, "Measurement of jet fragmentation in PbPb and pp collisions at $\sqrt{s_{NN}} = 2.76$ TeV," *Phys. Rev.* **C90** no. 2, (2014) 024908, arXiv:1406.0932 [nucl-ex].

[31] **ALICE** Collaboration, S. Acharya *et al.*, "Medium modification of the shape of small-radius jets in central Pb-Pb collisions at $\sqrt{s_{\mathrm{NN}}} = 2.76\,\mathrm{TeV}$," *JHEP* **10** (2018) 139, arXiv:1807.06854 [nucl-ex].

[32] A. Kurkela and U. A. Wiedemann, "Picturing perturbative parton cascades in QCD matter," *Phys. Lett.* **B740** (2015) 172–178, arXiv:1407.0293 [hep-ph].

[33] **JETSCAPE** Collaboration, Y. Tachibana *et al.*, "Jet substructure modification in a QGP from a multi-scale description of jet evolution with JETSCAPE," 2018. arXiv:1812.06366 [nucl-th].

[34] J. Casalderrey-Solana, Y. Mehtar-Tani, C. A. Salgado, and K. Tywoniuk, "New picture of jet quenching dictated by color coherence," *Phys. Lett.* **B725** (2013) 357–360, arXiv:1210.7765 [hep-ph].

[35] F. D'Eramo, M. Lekaveckas, H. Liu, and K. Rajagopal, "Momentum Broadening in Weakly Coupled Quark-Gluon Plasma (with a view to finding the quasiparticles within liquid quark-gluon plasma)," *JHEP* **05** (2013) 031, arXiv:1211.1922 [hep-ph].

[36] A. Ayala, I. Dominguez, J. Jalilian-Marian, and M. E. Tejeda-Yeomans, "Relating $\hat{q}$, η/s and ΔE in an expanding quark-gluon plasma," *Phys. Rev.* **C94** no. 2, (2016) 024913, arXiv:1603.09296 [hep-ph].

[37] **ALICE** Collaboration, B. Abelev *et al.*, "Long-range angular correlations on the near and away side in p-Pb collisions at $\sqrt{s_{NN}} = 5.02$ TeV," *Phys. Lett.* **B719** (2013) 29–41, arXiv:1212.2001 [nucl-ex].

[38] **ATLAS** Collaboration, G. Aad *et al.*, "Observation of Associated Near-Side and Away-Side Long-Range Correlations in $\sqrt{s_{NN}}$=5.02 TeV Proton-Lead Collisions with the ATLAS Detector," *Phys. Rev. Lett.* **110** no. 18, (2013) 182302, arXiv:1212.5198 [hep-ex].

[39] **CMS** Collaboration, S. Chatrchyan *et al.*, "Multiplicity and Transverse Momentum Dependence of Two- and Four-Particle Correlations in pPb and PbPb Collisions," *Phys. Lett.* **B724** (2013) 213–240, arXiv:1305.0609 [nucl-ex].

[40] **CMS** Collaboration, V. Khachatryan *et al.*, "Observation of Long-Range Near-Side Angular Correlations in Proton-Proton Collisions at the LHC," *JHEP* **09** (2010) 091, arXiv:1009.4122 [hep-ex].

[41] **CMS** Collaboration, V. Khachatryan *et al.*, "Evidence for collectivity in pp collisions at the LHC," *Phys. Lett.* **B765** (2017) 193–220, arXiv:1606.06198 [nucl-ex].

[42] C. Aidala *et al.*, "Measurement of long-range angular correlations and azimuthal anisotropies in high-multiplicity p+Au collisions at $\sqrt{s_{NN}} = 200$ GeV," *Phys. Rev.* **C95** no. 3, (2017) 034910, arXiv:1609.02894 [nucl-ex].

[43] X. Zhang and J. Liao, "Jet Quenching and Its Azimuthal Anisotropy in AA and possibly High Multiplicity pA and dA Collisions," arXiv:1311.5463 [nucl-th].

[44] C. Park, C. Shen, S. Jeon, and C. Gale, "Rapidity-dependent jet energy loss in small systems with finite-size effects and running coupling," *Nucl. Part. Phys. Proc.* **289-290** (2017) 289–292, arXiv:1612.06754 [nucl-th].

[45] K. Tywoniuk, "Is there jet quenching in ppb?," *Nuclear Physics A* **926** (2014) 85 – 91. http://www.sciencedirect.com/science/article/pii/S0375947414001055. IS2013.

[46] https://alice-publications.web.cern.ch/node/3655, 2018. https://alice-publications.web.cern.ch/node/3655.

[47] **ALICE** Collaboration, J. Adam *et al.*, "Centrality dependence of particle production in p-Pb collisions at $\sqrt{s_{\rm NN}}$= 5.02 TeV," *Phys. Rev.* **C91** no. 6, (2015) 064905, arXiv:1412.6828 [nucl-ex].

[48] **ALICE** Collaboration, J. Adam *et al.*, "Centrality dependence of charged jet production in p–Pb collisions at $\sqrt{s_{\rm NN}}$ = 5.02 TeV," *Eur. Phys. J.* **C76** no. 5, (2016) 271, arXiv:1603.03402 [nucl-ex].

[49] J. L. Nagle and W. A. Zajc, "Small System Collectivity in Relativistic Hadronic and Nuclear Collisions," *Ann. Rev. Nucl. Part. Sci.* **68** (2018) 211–235, arXiv:1801.03477 [nucl-ex].

[50] M. Cacciari, G. P. Salam, and G. Soyez, "The anti-k_t jet clustering algorithm," *JHEP* **04** (2008) 063, arXiv:0802.1189 [hep-ph].

[51] **ALICE** Collaboration, K. Aamodt *et al.*, "The ALICE experiment at the CERN LHC," *JINST* **3** (2008) S08002.

[52] **ALICE** Collaboration, B. B. Abelev *et al.*, "Performance of the ALICE Experiment at the CERN LHC," *Int. J. Mod. Phys.* **A29** (2014) 1430044, arXiv:1402.4476 [nucl-ex].

[53] **ALICE** Collaboration, K. Aamodt *et al.*, "Alignment of the ALICE Inner Tracking System with cosmic-ray tracks," *JINST* **5** (2010) P03003, arXiv:1001.0502 [physics.ins-det].

[54] J. Alme *et al.*, "The ALICE TPC, a large 3-dimensional tracking device with fast readout for ultra-high multiplicity events," *Nucl. Instrum. Meth.* **A622** (2010) 316–367, arXiv:1001.1950 [physics.ins-det].

[55] **ALICE** Collaboration, B. Abelev *et al.*, "Measurement of Event Background Fluctuations for Charged Particle Jet Reconstruction in Pb-Pb collisions at $\sqrt{s_{NN}} = 2.76$ TeV," *JHEP* **03** (2012) 053, arXiv:1201.2423 [hep-ex].

[56] **ALICE** Collaboration, P. Cortese *et al.*, "ALICE electromagnetic calorimeter technical design report,".

[57] J. Allen, C. Bernard, O. Bourrion, M. Chala, M. Del Franio, O. Driga, F. Fichera, N. Giudice, A. Grimaldi, P. Laloux, Q. Li, F. Librizzi, G. Liu, C. Loizides, G. Marcotte, S. Muggeo, J. F. Muraz, F. Noto, A. Orlandi, V. Petrov, F. Pompei, W. Qian, J. Rasson, S. Sakai, M. Salemi, M. Sharma, V. Sparti, J. S. Stutzmann, A. Timmons, A. Viticchie, M. Wang, X. Xiang, F. Zhang, J. Zhou, and X. Zhu, "ALICE DCal: An Addendum to the EMCal Technical Design Report Di-Jet and Hadron-Jet correlation measurements in ALICE," Tech. Rep. CERN-LHCC-2010-011. ALICE-TDR-14-add-1, Jun, 2010. https://cds.cern.ch/record/1272952.

[58] **ALICE** Collaboration, G. Dellacasa *et al.*, "ALICE technical design report of the photon spectrometer (PHOS),".

[59] ALICE Collaboration, *Technical Design Report on Forward Detectors: FMD, T0 and V0*, September, 2004.

[60] **ALICE** Collaboration, B. Abelev *et al.*, "Long-range angular correlations on the near and away side in p-Pb collisions at $\sqrt{s_{NN}} = 5.02$ TeV," *Phys. Lett.* **B719** (2013) 29–41, arXiv:1212.2001 [nucl-ex].

[61] M. Cacciari, G. P. Salam, and G. Soyez, "FastJet User Manual," *Eur. Phys. J.* **C72** (2012) 1896, arXiv:1111.6097 [hep-ph].

[62] S. Agostinelli, J. Allison, K. Amako, J. Apostolakis, H. Araujo, P. Arce, M. Asai, D. Axen, S. Banerjee, G. Barrand, F. Behner, L. Bellagamba, J. Boudreau, L. Broglia, A. Brunengo, H. Burkhardt, S. Chauvie, J. Chuma, R. Chytracek, G. Cooperman, G. Cosmo, P. Degtyarenko, A. Dell'Acqua, G. Depaola, D. Dietrich, R. Enami, A. Feliciello, C. Ferguson, H. Fesefeldt, G. Folger, F. Foppiano, A. Forti, S. Garelli, S. Giani, R. Giannitrapani, D. Gibin, J. G. Cadenas, I. González, G. G. Abril, G. Greeniaus, W. Greiner, V. Grichine, A. Grossheim, S. Guatelli, P. Gumplinger, R. Hamatsu, K. Hashimoto, H. Hasui, A. Heikkinen, A. Howard, V. Ivanchenko, A. Johnson, F. Jones, J. Kallenbach, N. Kanaya, M. Kawabata, Y. Kawabata, M. Kawaguti, S. Kelner, P. Kent, A. Kimura, T. Kodama, R. Kokoulin, M. Kossov, H. Kurashige, E. Lamanna, T. Lampén, V. Lara, V. Lefebure, F. Lei, M. Liendl, W. Lockman, F. Longo, S. Magni, M. Maire, E. Medernach, K. Minamimoto, P. M. de Freitas, Y. Morita, K. Murakami, M. Nagamatu, R. Nartallo, P. Nieminen, T. Nishimura, K. Ohtsubo, M. Okamura, S. O'Neale, Y. Oohata, K. Paech, J. Perl, A. Pfeiffer, M. Pia, F. Ranjard, A. Rybin, S. Sadilov, E. D. Salvo, G. Santin, T. Sasaki, N. Savvas, Y. Sawada, S. Scherer, S. Sei, V. Sirotenko, D. Smith, N. Starkov, H. Stoecker, J. Sulkimo, M. Takahata, S. Tanaka, E. Tcherniaev, E. S. Tehrani, M. Tropeano, P. Truscott, H. Uno, L. Urban, P. Urban, M. Verderi, A. Walkden, W. Wander, H. Weber, J. Wellisch, T. Wenaus, D. Williams, D. Wright, T. Yamada, H. Yoshida, and D. Zschiesche, "Geant4—a simulation toolkit," *Nuclear Instruments and Methods in Physics Research Section A:*

Accelerators, Spectrometers, Detectors and Associated Equipment **506** no. 3, (2003) 250 – 303. http://www.sciencedirect.com/science/article/pii/S0168900203013688.

[63] J. Allison, K. Amako, J. Apostolakis, P. Arce, M. Asai, T. Aso, E. Bagli, A. Bagulya, S. Banerjee, G. Barrand, B. Beck, A. Bogdanov, D. Brandt, J. Brown, H. Burkhardt, P. Canal, D. Cano-Ott, S. Chauvie, K. Cho, G. Cirrone, G. Cooperman, M. Cortés-Giraldo, G. Cosmo, G. Cuttone, G. Depaola, L. Desorgher, X. Dong, A. Dotti, V. Elvira, G. Folger, Z. Francis, A. Galoyan, L. Garnier, M. Gayer, K. Genser, V. Grichine, S. Guatelli, P. Guèye, P. Gumplinger, A. Howard, I. Hřivnáčová, S. Hwang, S. Incerti, A. Ivanchenko, V. Ivanchenko, F. Jones, S. Jun, P. Kaitaniemi, N. Karakatsanis, M. Karamitros, M. Kelsey, A. Kimura, T. Koi, H. Kurashige, A. Lechner, S. Lee, F. Longo, M. Maire, D. Mancusi, A. Mantero, E. Mendoza, B. Morgan, K. Murakami, T. Nikitina, L. Pandola, P. Paprocki, J. Perl, I. Petrović, M. Pia, W. Pokorski, J. Quesada, M. Raine, M. Reis, A. Ribon, A. R. Fira, F. Romano, G. Russo, G. Santin, T. Sasaki, D. Sawkey, J. Shin, I. Strakovsky, A. Taborda, S. Tanaka, B. Tomé, T. Toshito, H. Tran, P. Truscott, L. Urban, V. Uzhinsky, J. Verbeke, M. Verderi, B. Wendt, H. Wenzel, D. Wright, D. Wright, T. Yamashita, J. Yarba, and H. Yoshida, "Recent developments in geant4," *Nuclear Instruments and Methods in Physics Research Section A: Accelerators, Spectrometers, Detectors and Associated Equipment* **835** (2016) 186 – 225. http://www.sciencedirect.com/science/article/pii/S0168900216306957.

A The ALICE Collaboration